Microfluidic Immunoassay Devices as Next-Generation Cancer and Medical Diagnostics Platform

13

Toshihiro Kasama, Yoshinobu Baba, and Manabu Tokeshi

13.1 Introduction

Immunoassays are applied for medical diagnostics, food safety testing, drug discovery, biological researches, etc. (Wild 2005) and they show some of the most remarkable activities in the field of lab-on-a-chip systems and micro total analysis systems (Bange et al. 2005; Chin et al. 2007; Henares et al. 2008; Tachi et al. 2007). Miniaturization of immunoassay systems enables rapid and highly sensitive analysis with a small amount of sample and reagents.

Since the first study of chip-based immunoassay (Chiem and Harrison 1997), immobilization of antibody on the surface of microbeads has contributed to the improvement of detection sensitivity and assay time (Sato et al. 2000, 72; Moorthy et al. 2004; Haes et al. 2006; Shin et al. 2007; Thompson and Bau 2010). This is called the bead-bed format. We have published papers on the subject of the

T. Kasama (✉)
School of Engineering, The University of Tokyo, Tokyo, Japan

Graduate School of Engineering, Nagoya University, Nagoya, Japan
e-mail: kasama.toshihiro@kk.alumni.u-tokyo.ac.jp

Y. Baba
Graduate School of Engineering, Nagoya University, Nagoya, Japan

ImPACT Research Center for Advanced Nanobiodevices, Nagoya University, Nagoya, Japan

Graduate School of Medicine, Nagoya University, Nagoya, Japan

National Institute of Advanced Industrial Science and Technology, Takamatsu, Japan
e-mail: babaymtt@apchem.nagoya-u.ac.jp

M. Tokeshi
ImPACT Research Center for Advanced Nanobiodevices, Nagoya University, Nagoya, Japan

Faculty of Engineering, Hokkaido University, Sapporo, Japan
e-mail: tokeshi@eng.hokudai.ac.jp

P. Chandra et al. (eds.), *Next Generation Point-of-care Biomedical Sensors Technologies for Cancer Diagnosis*, DOI 10.1007/978-981-10-4726-8_13

bead-bed format immunoassay devices, in which the capability of this format to detect human disease markers has been demonstrated (Sato et al. 2001, 2002, 2004; Kakuta et al. 2006; Ohashi et al. 2009; Ihara et al. 2010). However, there exist some difficulties for this format in liquid handling, though highly sensitive detection and rapid assay are achieved. In order to pack the microbeads inside the microchannel, it is necessary to apply relatively high pressure. In addition, the removal of bubbles from liquid is difficult. Therefore, the development of novel immunoassay chips is desired for clinical applications such as point-of-care (POC) testing (Delamarche et al. 2005; Linder et al. 2005; Hosokawa et al. 2006; Gervais and Delamarche 2009). On the other hand, three-dimensional (3-D) hydrogel-based immunoassay chips have been reported (Zubtsov et al. 2006; Sung et al. 2009). They showed that the immobilization of antibodies within 3-D hydrogel structures offers several advantages, such as high immobilization capacity and high antibody activity, over 2-D immobilization.

In this chapter, we introduce two types of new immunoassay microdevices, both of which can overcome difficulties mentioned above. One is 3-D hydrogel structures holding antibody-immobilized microbeads. Another device is 3-D hydrogel structures with chemically bonded antibodies.

13.2 Microbead-Embedded Immunoassay Devices

13.2.1 Fabrication Procedure of Microbead-Embedded Immunoassay Devices

Antibody-immobilized beads were prepared with polystyrene beads (1 μm in diameter) and antibody solution in a 1.5 mL microtube. The antibody solution was added to the microbeads, and the suspension was rotated gently at room temperature, followed by overnight incubation at 4 °C. After the incubation, the antibodies were immobilized on the microbeads, but there was space among the antibody molecules for nonspecific adsorption of proteins such as antigen and detection antibody. In order to prevent nonspecific adsorption, the microbeads were immersed in 1% BSA for 45 min at room temperature.

Photocross-linkable prepolymer, photoinitiator, and Millipore water were mixed in another 1.5 mL microtube and the mixture was stirred using a vortex mixer. The mixture was added to the antibody-immobilized microbead solution. Then, the mixture was stirred gently at room temperature. This solution was used to fabricate microbead-embedded immunoassay devices. Fabrication steps of the devices are shown in Fig. 13.1. First, 250 nL of the solution was injected into the microchannel by using a pipette. Second, UV light (365 nm, 20 mW) was irradiated through a photomask covering the microchannel. This process took approximately 10 s. The exposed areas became hydrogel structures which included many antibody-immobilized microbeads. Third, the non-polymerized solution was sucked by using a vacuum pump, and the surface of the microchannel was flushed

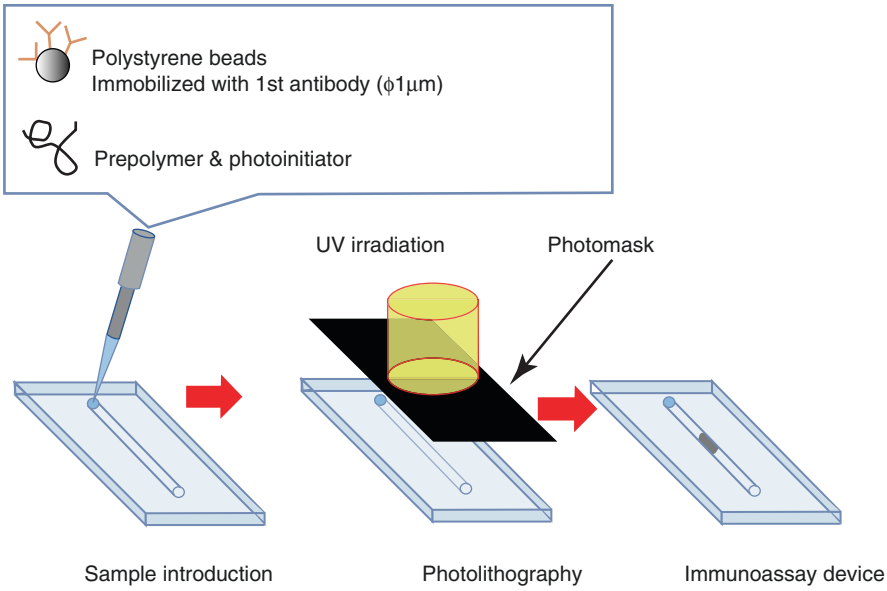

Fig. 13.1 Fabrication steps of the microbead-embedded immunoassay devices

with PBS. Finally, 1% BSA in PBS was injected and then kept in the microchannel for 1 h at room temperature. BSA prevented nonspecific binding of antigens and detection antibodies to the surface of the microchannel and hydrogel structures. After removing the BSA solution, the microchannel was flushed with PBS. Although the hydrogel structures were physically fixed between the roof and the floor of the microchannel, they did not move or break during the immunoassay.

13.2.2 Assay Procedures

First, 250 nL of the sample solution was injected into the microchannel with a pipette. After incubation, free antigen molecules in the sample solution were sucked with an aspirator, and then the microchannel was flushed three times with PBS. Second, 250 nL (1 μg mL^{-1}) of the fluorescent-labeled detection antibody solution was injected into the microchannel. After the incubation, the microchannel was flushed three times with PBS to remove the free fluorescent-labeled secondary antibody molecules. Finally, the fluorescence signal from the microbeads in hydrogel structures was detected by using a fluorescence microscope equipped with a CCD camera and three lasers (488, 532, and 632.8 nm). By using ImageJ software, the fluorescent intensity per unit area was calculated for each hydrogel structure.

13.2.3 Immuno-Pillar Device

Firstly, we developed pillar-like hydrogel structure by using a photomask shown in Fig. 13.2. We call this immunoassay chip the immuno-pillar device (Ikami et al. 2010). Each immuno-pillar has a dimension of 200 μm in diameter and 40 μm in height. The arrangement of five immuno-pillars is shown in Fig. 13.3.

13.2.3.1 Immunoassay of Disease Markers

First, we evaluated the performance of the immuno-pillar device for standard C-reactive protein (CRP) solutions (1% BSA in PBS). CRP is a well-known disease marker relating cardiac events and inflammation. The calibration curves for

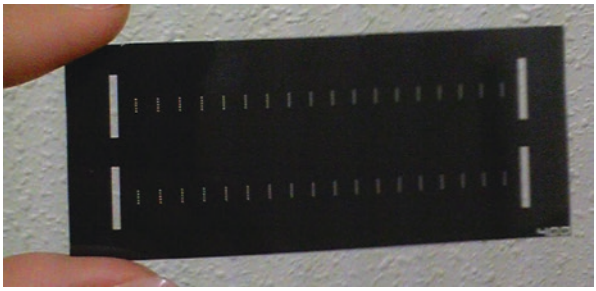

Fig. 13.2 Picture of photomask prepared for fabricating the immuno-pillar devices

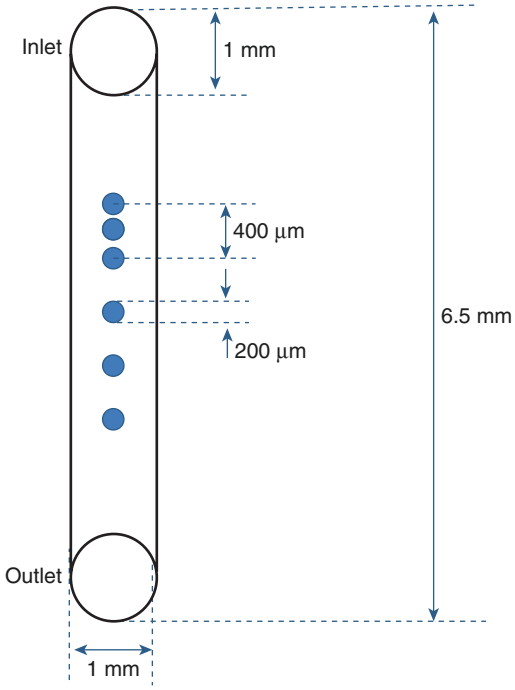

Fig. 13.3 Schematic representation of the immuno-pillar device

standard CRP solutions are shown in Fig. 13.4a–c. In our assay procedures, total assay time was calculated by adding all the times for the incubations, washings, and detection. The fluorescence intensity represents the average of the fluorescence signal intensities of 3–5 immuno-pillars. The error bar denotes their standard deviation. The background is the sum of the autofluorescence of plastic substrate, antibody-immobilized microbeads, and UV curable resin. The total assay times were 4 min, 8 min, and 12 min, respectively. Despite the very short assay times, fluorescence signal and CRP concentration have positive correlation. The calibration curve of (B) (total assay time: 8 min) was very similar to that of (A) (12 min). From (A), (B), and (C) (4 min), the limit of detection (LOD), which gave a signal at 3 SDs (standard deviations) above the background, was estimated to be 100 pg mL^{-1}; the slope of the calibration curve of (C) was gentle. The immuno-pillar devices demonstrated the ability to detect disease marker with high sensitivity and rapidity in spite of easy assay procedure. For actual diagnosis of several diseases, the cutoff values of CRP concentration are higher than 100 pg mL^{-1} (Gabay and Kushner 1999). Also, we could change the detection range of the immuno-pillar device by using a lower concentration of fluorescence-labeled secondary antibody or a lower power of the excitation laser beam (data not shown). In particular, shifting the detection range to higher sample concentrations is easier than that to lower concentrations. The features of the immuno-pillar device of rapid assay and high sensitivity were derived from the immuno-pillar itself and the 1 μm diameter polystyrene microbeads for the immobilization of capture antibodies. The pore size of the immuno-pillars was likely 100 nm or more because the fluorescence beads with diameter of 100 nm leaked from the immuno-pillars in our preliminary experiments. The diffusion kinetics of the antigen and antibody within the immuno-pillars was not slow (Fig. 13.5). Therefore, protein molecules such as the antigen and antibody could easily penetrate into the immuno-pillars and could diffuse within the immuno-pillars. According to our calculation for the present experimental conditions, the number of microbeads within the immuno-pillar was estimated to be about 32,700. By using the surface of these microbeads, the number of reaction sites for an antigen–antibody reaction was dramatically increased.

Next, we tested the performance of the immuno-pillar device for serum samples which were spiked with the known concentrations of CRP. Figure 13.4 d–f shows the calibration curves for serum samples with CRP. The immuno-pillar devices showed good performance also for serum samples. Influence of proteins in the serum may cause the scattering of the signal intensity in the high-concentration region. The LOD for the total assay time of 4, 8, and 12 was 100 pg mL^{-1}.

In addition, we also evaluated the performance of the immuno-pillar devices for the standard and serum samples of alpha-fetoprotein (tumor marker) and prostate-specific antigen (prostate cancer marker). These results are summarized in Table 13.1. In summary, we can conclude that the immuno-pillar devices had great potential for tests of serum samples and would be suitable as an immunoassay device for POC diagnostics because it was quick, had high sensitivity, was easy to use, and needed only small sample and reagent volumes.

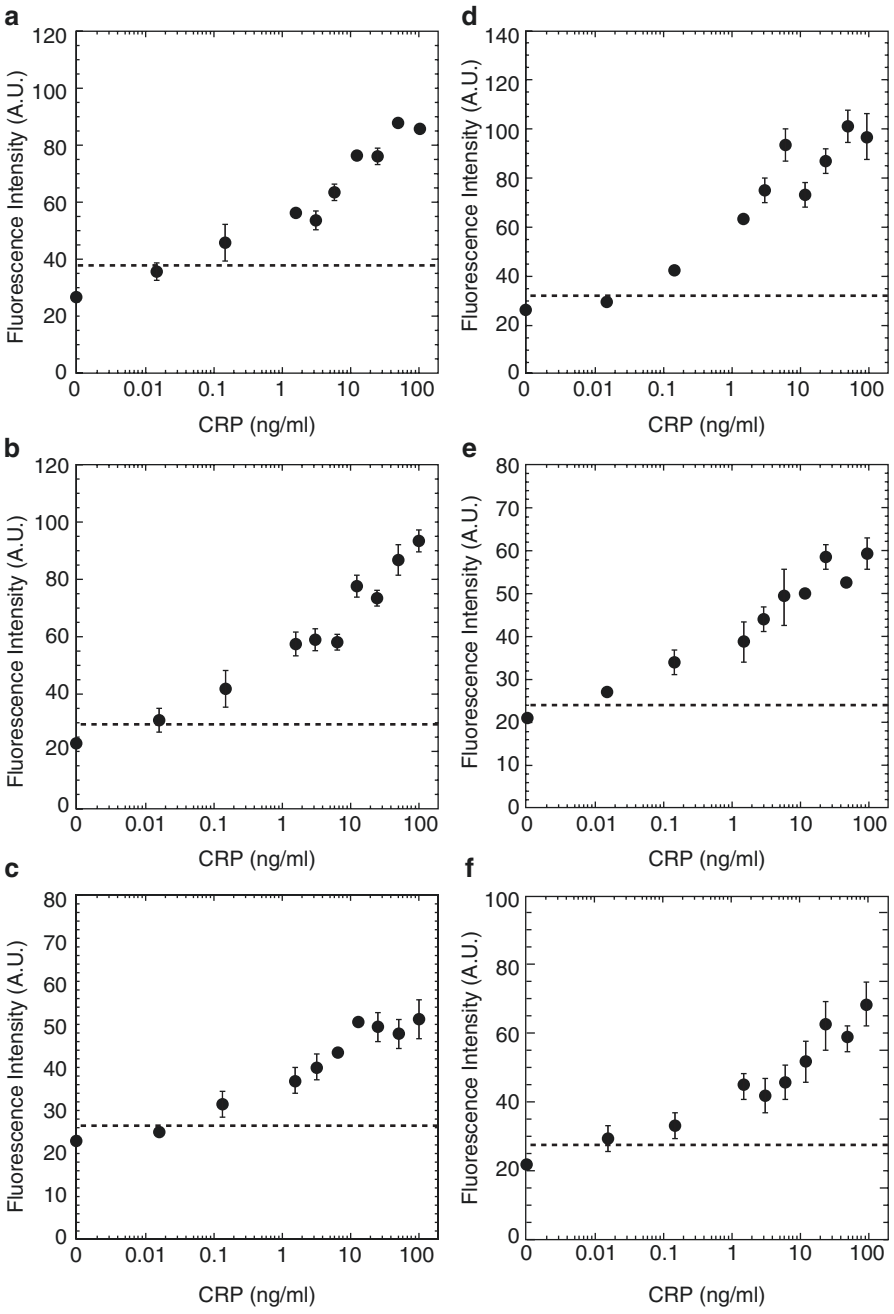

Fig. 13.4 Calibration curves obtained with CRP of standard samples (**a**–**c**) and of serum samples (**d**–**f**) (adapted from reference Ikami et al. (2010)). Total assay times were (**a**) 12 min, (**b**) 8 min, (**c**) 4 min, (**d**) 12 min, (**e**) 8 min, and (**f**) 4 min. The *dashed line* represents the signal level at 3 SDs above the background

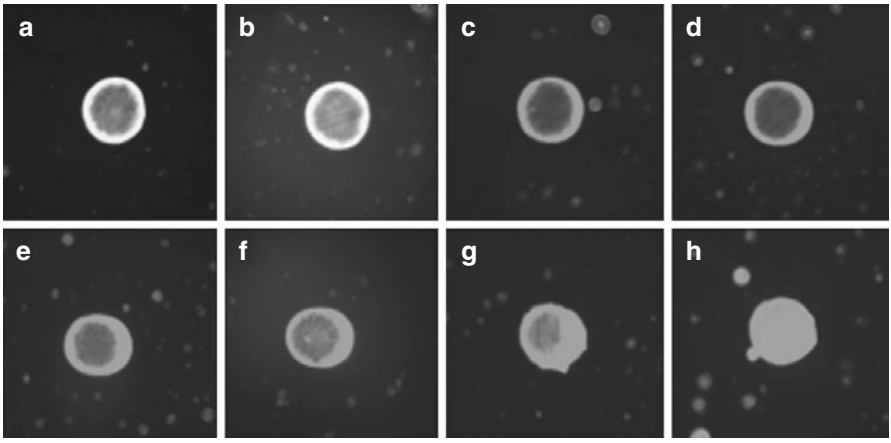

Fig. 13.5 Fluorescence images of the immuno-pillar at the fluorescence-labeled antibody immersion time of (**a**) 40, (**b**) 60, (**c**) 80, (**d**) 100, (**e**) 120, (**f**) 140, (**g**) 160, and (**h**) 180 s (reproduced with permission from reference Ikami et al. (2010))

Table 13.1 Detection sensitivity of the immuno-pillar devices (adapted from reference Ikami et al. (2010))

Sample		Tota assay time		
		4 min	8 min	12 min
CRP	In 1% BSA-PBS	~100 pg mL^{-1}	~100 pg mL^{-1}	~100 pg mL^{-1}
	In serum	~100 pg mL^{-1}	~100 pg mL^{-1}	~100 pg mL^{-1}
AFP[a]	In 1% BSA-PBS	~100 pg mL^{-1}	~100 pg mL^{-1}	~100 pg mL^{-1}
	In serum	~1 ng mL^{-1}	~1 ng mL^{-1}	~100 pg mL^{-1}
PSA[a]	In 1% BSA-PBS	~5 ng mL^{-1}	~1 ng mL^{-1}	~100 pg mL^{-1}
	In serum	~5 ng mL^{-1}	~5 ng mL^{-1}	~100 pg mL^{-1}
Triplex	In serum	—	—	~100 pg mL^{-1}

[a]In the assay of AFP and PSA, the concentration of the fluorescent-labeled detection antibody solution was 50 μg mL^{-1} and 50 μg mL^{-1}, respectively

13.2.3.2 Multiplex Immunoassay of Disease Markers

The immuno-pillar devices are also available to perform multiplex assay. For example, if the immuno-pillars hold three kinds of microbeads (three different antibodies are immobilized), a triplex assay becomes possible. Schematic illustration of the immuno-pillar device for the triplex assay is depicted in Fig. 13.6a. Fabrication process of this immuno-pillar device is the same as that of the above-mentioned devices. Therefore, the number of each kind of microbeads in the immuno-pillar is one-third, ca. 10,000. We fabricated a suitable immuno-pillar device and performed triplex simultaneous assay for CRP, AFP, and PSA. 250 nL of serum solution which was spiked with CRP, AFP, and PSA was used as the sample. 250 nL of the mixture solution of fluorescence dye-labeled antibodies was used as the detection antibody solution. The incubation time was constant at 5 min. Thus, the assay for one sample

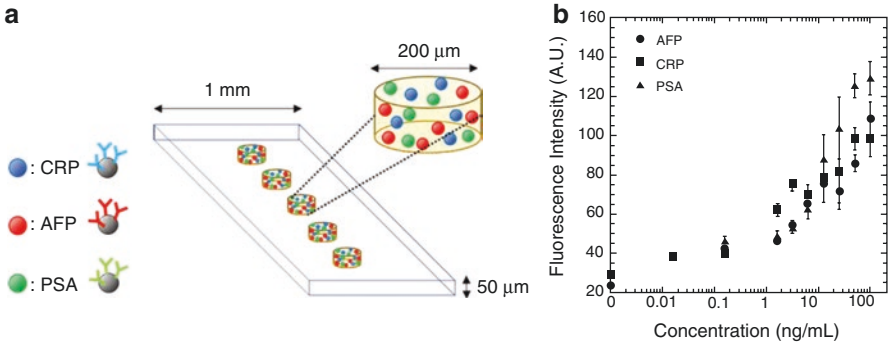

Fig. 13.6 (**a**) Simplified schematic of the immuno-pillar device for the triplex assay. (**b**) Calibration curves of CRP, AFP, and PSA (adapted from reference Ikami et al. (2010))

was finished in 15 min. The results of the multiplex assay are shown in Fig. 13.6b. All three calibration curves showed the positive correlations between the fluorescence signal and the sample concentration, and the LOD for each was 100 pg mL^{-1}. It should be noted that the LODs for three markers in the multiplex assay were almost the same as that of the single assay. From this analysis, we could conclude that the immuno-pillar devices had great potential also for multiplex assay of serum samples. Moreover, optimization of the number of microbeads and/or the concentrations of detection antibodies may lead to the shortening of assay time.

13.2.3.3 Immunoassay of Toxins in Food

Immuno-pillar devices could be applied to detect toxins in dairy products (Jin et al. 2013). Here we attempt to detect staphylococcal enterotoxins (SEs) in milk by using chicken immunoglobulin IgY anti-SE antibody as capture antibody. IgY antibodies, unlike mammalian IgG antibodies, do not combine with protein A because they possess a different structure of the Fc region, thereby avoiding nonspecific reactivity against *Staphylococcus aureus*. We performed detection tests against SEs in milk. The total assay time was approximately 12 min. The calibration curves for SEs are summarized in Fig. 13.7. These results show that fluorescence intensities increased in a dose-dependent manner for SEs (0–100 ng/mL) in milk. In all cases, each immuno-pillar device could detect the corresponding SEs with high sensitivity. The LODs for SEA, SEB, SEC, SED, and SEE are summarized in Table 13.2. High specificity of the SE immuno-pillar devices was confirmed by measuring the cross-reactivity against the comparative antigens of 100 ng mL^{-1}.

13.2.3.4 Multiplex Immunoassay of Toxins in Food

Several kinds of SEs often coexist in polluted foods. Therefore, we evaluated the ability of the immuno-pillar devices to detect SEA, SEB, and SED simultaneously (Kasama et al. 2015a). These are the three worst factors of SE poisoning. In order to simulate contaminated milk, standard, native SEs with more than 95% purity were diffused in commercially available milk. The resulting calibration plots for SEA,

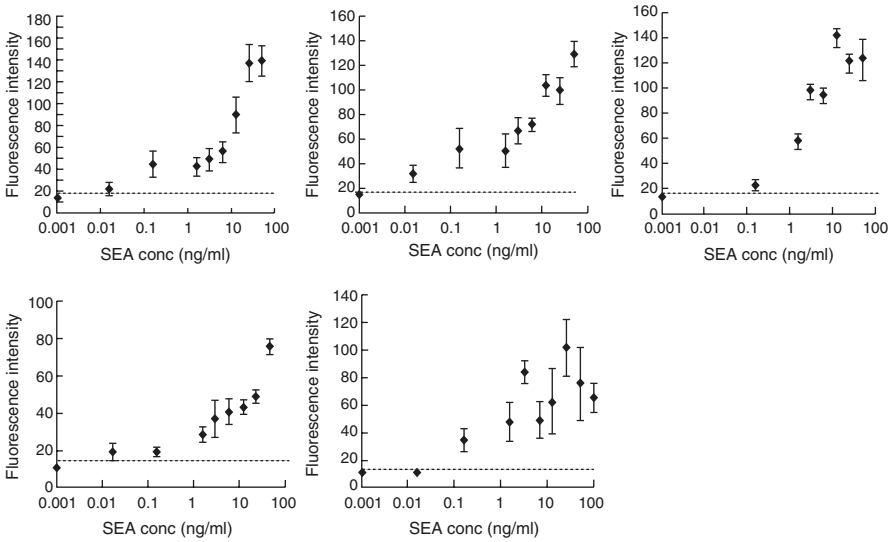

Fig. 13.7 Calibration plots of standard SEs in milk (reproduced with permission from reference Jin et al. (2013)). All tests were performed in triplicate, and *error bars* show standard deviation calculated from fluorescence intensities of 3–5 immuno-pillars. *Dashed lines* represent the signal levels at 3 SDs above the background

Table 13.2 Detection limits of immuno-pillar device (ng mL^{-1}) (adapted from reference Jin et al. (2013))

	SEA	SEB	SEC	SED	SEE
Immuno pillar device (in PBS)	0.01	0.1	0.1	0.1	0.1
Immuno pillar device (in milk)	0.1	0.01	0.1	0.1	0.1

SEB, and SED were obtained (Fig. 13.8). The tests for three replicates per sample were performed. The values and SDs of the fluorescence intensity were calculated from these results. The LOD for each SE was calculated to be 15.6 pg mL^{-1}, which is lower than not only those of common SE detection methods (Jin et al. 2013; Rose et al. 1989; Kuang et al. 2013), but also those of the immuno-pillar devices for single assays of SEA and SED (Jin et al. 2013). Relaxation of self-quenching (Chen and Knutson 1988) enhances fluorescence intensity, resulting in lower LODs. In the immuno-pillars, the antibody-immobilized microbeads formed clusters via hydrophobic interaction between the antibodies. In the case of multiplex immunoassay devices, microbead clusters were composed of three kinds of microbeads supporting each anti-SE antibody. Consequently, the distance between the same fluorescence-labeled antibodies was relatively extended in the multiplex immunoassay devices. The LOD for each SE is much lower than the lowest SE concentration in major food poisoning outbreaks (380 pg mL^{-1}) (Asao et al. 2003). Therefore, contaminated food that may potentially cause a food poisoning outbreak could be immediately identified by immunoassay by using the immuno-pillar devices.

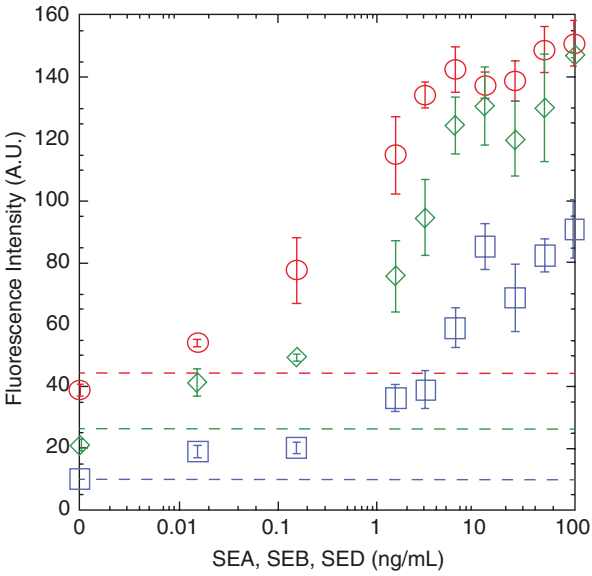

Fig. 13.8 Calibration plots for SEA (*red*), SEB (*blue*), and SED (*green*) (reproduced with permission from reference Kasama et al. (2015a)). The detection limits are represented by the *dashed lines* and are estimated as 3 SD above the backgrounds

13.2.4 Immuno-Wall Device

13.2.4.1 Immunoassay of Disease Markers

In order to improve the efficiency of bound-free (BF) separation, we modified the structure of immuno-pillars. Here, we propose immuno-wall device which has a long and thin hydrogel object inside a microchannel (Fig. 13.9) (Kasama et al. 2014). Unreacted antigens and fluorescence-labeled antibodies were completely removed by just immersing the device in a washing buffer (PBS with 0.5% Tween 20) for 1 min. In addition, the long structure also allowed us to analyze fluorescence intensity by using inexpensive desktop fluorescence scanner instead of expensive fluorescence microscopes.

First, we compared the efficiencies of BF separation of the immuno-wall and immuno-pillar devices. We prepared DyLight 650-conjugated anti-rabbit IgG antibody solution (50 μg mL^{-1}), which did not react to the antibody immobilized on the microbead surface. The devices underwent immersion in the solution (30 s) and the washing buffer (several minutes). After that, fluorescence intensity was measured by using a fluorescence microscope. The results are shown in Fig. 13.10. This figure shows that the unreacted fluorescence-labeled antibodies exited from the immuno-wall within 1 min by simply immersing the device into a washing buffer. In contrast, fluorescence-labeled antibodies could not exit from the immuno-pillar even after 9-min immersion. In order to completely remove non-reacted antibodies from immuno-pillars, it is necessary to squeeze the immuno-pillar by aspiration.

The long structure of the immuno-wall devices allowed us to determine fluorescence intensity by simple fluorescence scanner. Recently, we have developed microchip-optimized fluorescence scanner (Fig. 13.11). This scanner scanned on a line of 20 mm length and 100 μm width and obtained the profile of fluorescence

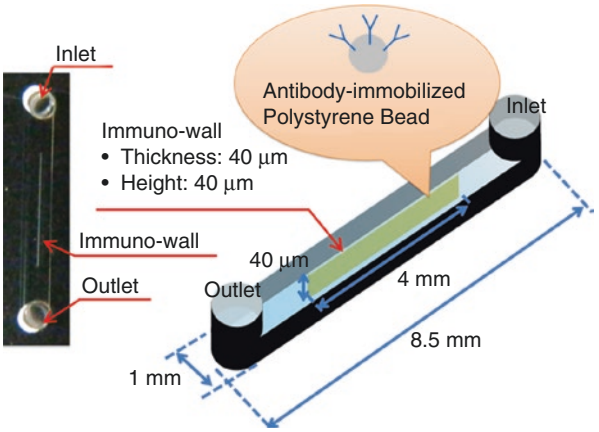

Fig. 13.9 Photograph and schematic of the immuno-wall device (reproduced with permission from reference Kasama et al. (2014)). Free antigens and fluorescence-labeled antibodies were easily removed from both sides of the immuno-wall

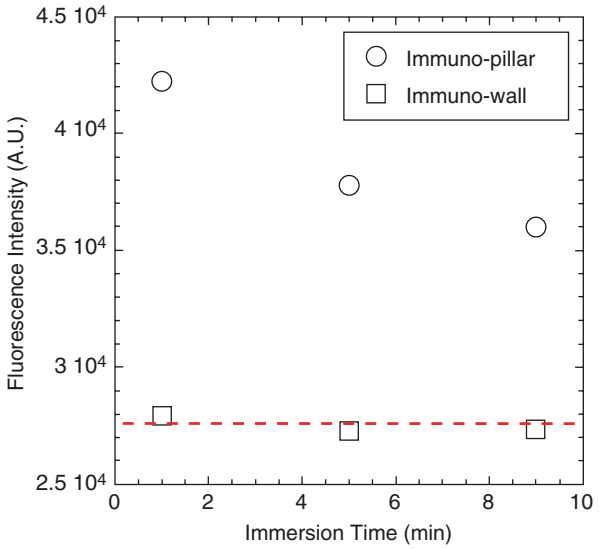

Fig. 13.10 Efficiencies of bound-free separation. The *dashed line* shows the autofluorescence intensity of the immuno-pillar and immuno-wall devices (reproduced with permission from reference Kasama et al. (2014))

intensity within 1 min. It was easy to scan across the immuno-wall devices having the dimension of 4 mm in length. In contrast, it was difficult to scan the immuno-pillar devices as small as 200 μm in diameter because this reader had no objective lens.

By using the immuno-wall devices and the fluorescence scanner, CRP assays for human sera were performed. The total assay time was 10 min. CRP in human sera were quantitatively analyzed and the calibration curve was obtained (Fig. 13.12). The fluorescence intensity was obtained by averaging the fluorescence signal intensities of 3–5 areas of the immuno-wall. We achieved the LOD of 10 ng mL^{-1}. In addition, the present immunoassay system provided good quantitative capability between 10 ng/mL and 10 μg mL^{-1}, offering the application possibility for rapid CRP test.

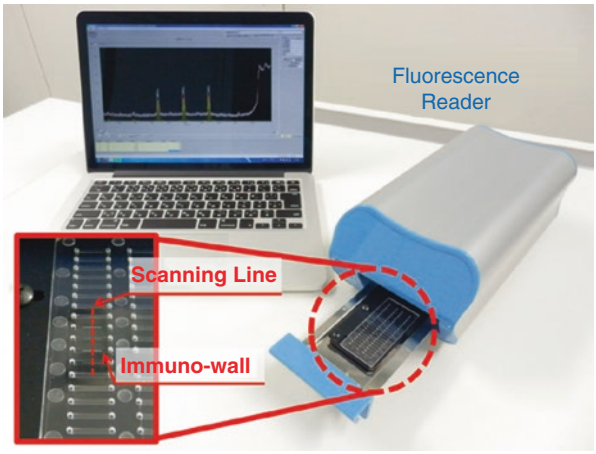

Fig. 13.11 Photograph of the fluorescence reader. Specification of the reader is as follows: weight = 2.1 kg, dimension ($W \times H \times D$) = 130 × 95 × 260 (mm), and maximal excitation wavelength = 637 nm. In the inset, the *dashed line* represents the scanning area (length = 20 mm, width = 100 μm) (reproduced with permission from reference Kasama et al. (2014))

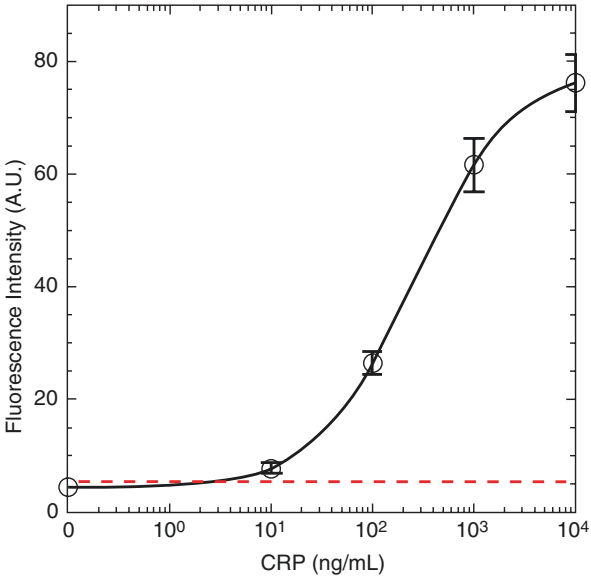

Fig. 13.12 Calibration curve for CRP in human serum. Sigmoidal curve was calculated by the four-parameter logistic equation. The immunoassay was carried out three times at each concentration (reproduced with permission from reference Kasama et al. (2014))

13.3 Immuno-Wall Devices with Chemically Bonded Antibodies

13.3.1 Fabrication Procedure of Immunoassay Devices with Chemically Bonded Antibodies

Until now, we presented the immuno-pillar devices and immuno-wall devices which held antibody-immobilized microbeads in their pores. In this section, we fabricate the immuno-wall devices with another photocross-linkable polymer, BIOSURFINE®-AWP (Toyo Gosei Co., Ltd.), which has pendant azide group. Picture and schematic of the

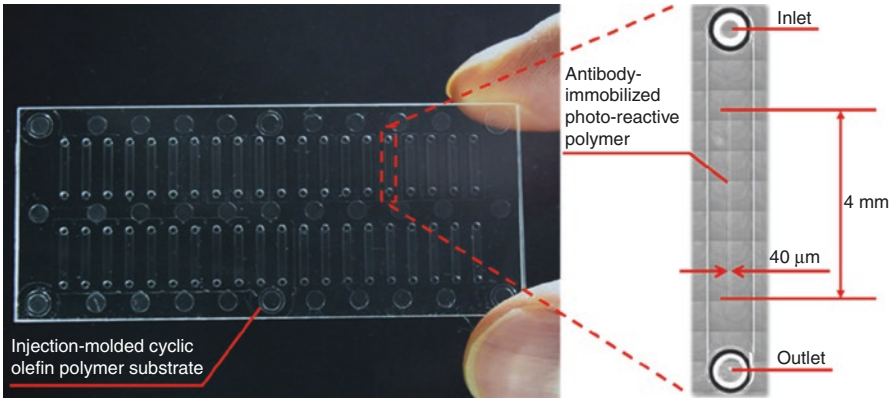

Fig. 13.13 Photograph of the immuno-wall device made with azido-unit pendant polymer (reproduced with permission from reference Kasama et al. (2015b))

immuno-wall device made with BIOSURFINE®-AWP is shown in Fig. 13.13. The device fabrication process is as follows. High-concentration (10 mg mL^{-1}) streptavidin in PBS was mixed with an equal volume of BIOSURFINE®-AWP in a microtube. The mixture was introduced into the microchannel by using the pipette. Then, the mixture was irradiated with UV light (320 nm, 20 mW) for 5 s through a photomask covering the microchannel. The irradiated BIOSURFINE®-AWP was cross-linked each other. At the same time, streptavidin molecules were photo-immobilized to the BIOSURFINE®-AWP. After the UV irradiation, the uncured BIOSURFINE®-AWP was sucked by using an aspirator. Then, immuno-wall remained at the center of the microchannel. Finally, the microchannel was washed with washing buffer. In order to immobilize capture antibody, 1 μL of biotinylated antibody solution was introduced into the microchannel and the device was settled for 60 min at room temperature. Although the diffusion of proteins including IgG antibody was observed in the immuno-wall, mostly analytes were captured at the side surface of the immuno-wall because of ultrahigh-density immobilization of capture antibody. On the other hand, large substances including cell debris could not penetrate the immuno-wall.

13.3.2 Precision Medicine of Lung Cancer

Lung cancer is the leading cause of cancer-related mortality worldwide. Approximately 85% of lung cancers are classified as non-small-cell lung cancer (NSCLC) (Ferlay et al. 2015). Somatic mutations of epidermal growth factor receptor (EGFR) are detected in approximately 10–16% of NSCLC patients in the United States and Europe (Rosell et al. 2009) and 30–50% in Asia (Sequist et al. 2007). Approximately 90% of these mutations are the substitution of leucine 858 by arginine in exon 21 (L858R point mutation) (Sequist et al. 2007) and the in-frame deletions in exon 19, especially the E746-A750 deletion (Sequist et al. 2007). Several studies revealed that these mutations have sensitivity to EGFR-tyrosine kinase inhibitors (TKIs) (Lynch et al. 2004; Paez et al. 2004). Therefore, EGFR mutation testing in the clinical setting has been important. Direct sequencing of PCR

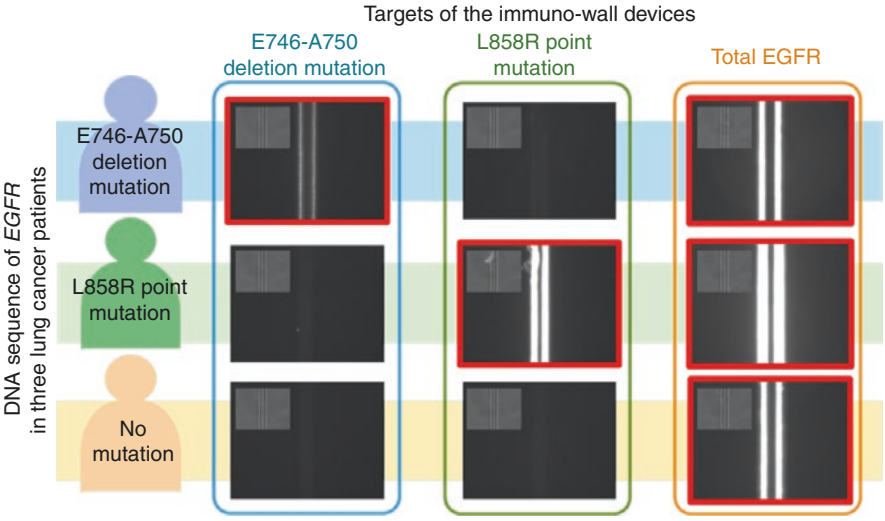

Fig. 13.14 Immunoassay results (reproduced with permission from reference Kasama et al. (2015b)). Bright-field images (*insets*) and fluorescence images of the immuno-wall devices are shown. The *red frames* of pictures show the results being positive. The side surfaces of immuno-walls exposed to the sediment lysates emitted fluorescence signals

products is one of the commonly used methods worldwide. However, its clinical application is limited due to the sensitivity depending on the proportion of tumor cells in the specimens.

By using the immuno-wall devices, the sandwich-type fluorescence immunoassay procedure was performed for the sediment lysates obtained from pleural effusion samples of three NSCLC patients. Their tumors had E746-A750 deletion-mutated EGFR, L858R point-mutated EGFR, or wild-type EGFR, respectively. The sediments in the pleural effusion were gathered by centrifugation, and then lysed with lysis buffer. Mutated EGFR-specific antibodies and total-EGFR antibody were immobilized to the immuno-walls. Another total-EGFR antibody was employed as detection antibody.

The immunoassay results are summarized in Fig. 13.14. Total assay time was less than 20 min. We can obviously recognize that the devices detected mutated EGFRs specifically. This means that the patients having responses to the EGFR-TKI are successfully distinguished.

13.3.3 Precision Surgery of Brain Tumors

Since the glioma tends to infiltrate into the normal brain tissue, it is difficult to define the edges of glioma. Therefore, the gliomas are not fully resectable, resulting in recurrence and eventual fatality. Because R132H mutation in IDH1 is observed in patients with grade II and III gliomas with approximately 65% (Suzuki et al. 2015; Gorovets et al. 2012; Hartmann et al. 2009; Parsons et al. 2008; Arita et al. 2015; Horbinski 2013), IDH1 mutation testing should help us to define the tumor boundary from the normal brain. However, the current methods for analyzing the genetic

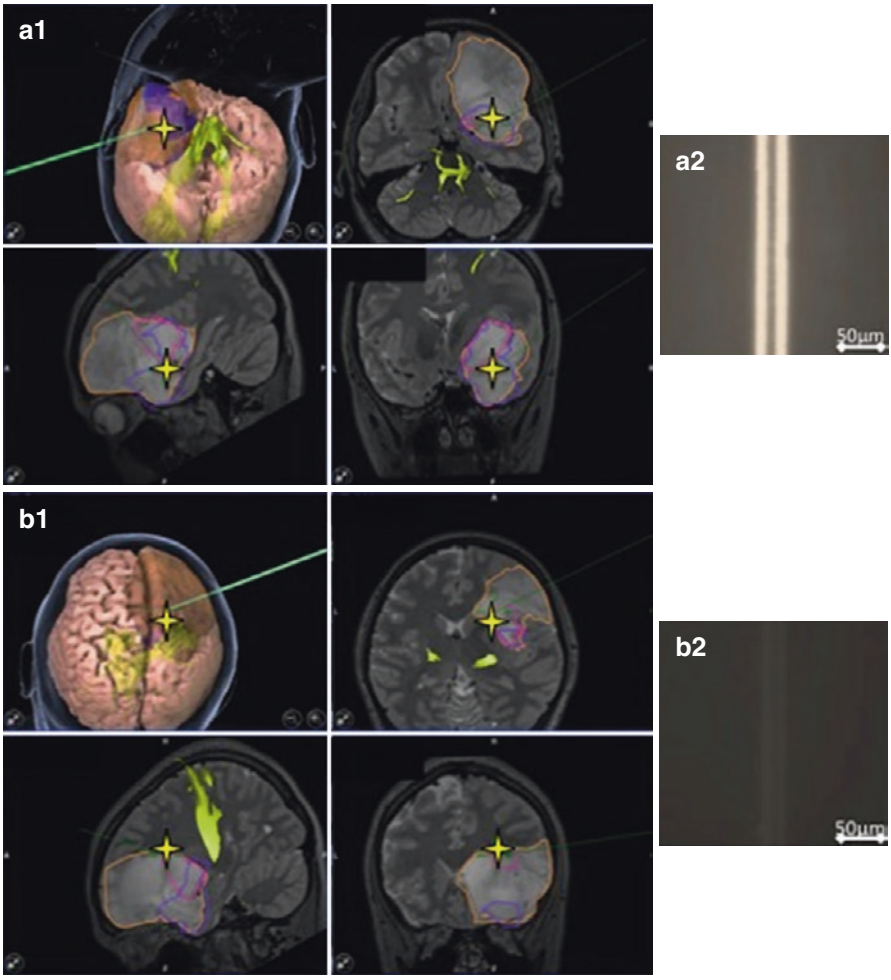

Fig. 13.15 Tumor boundary detection using the immuno-wall devices (adapted from reference Yamamichi et al. (2016)). The tumor region in a patient was roughly estimated by the magnetic resonance imaging before tumor removal surgery (A1 and B1). Two specimens were collected (*stars* in A1 and B1). A specimen obtained from the center of the tumor (*star* in A1) tested positive in the assay using the immuno-wall device (A2). On the other hand, a specimen obtained from the edge of the tumor (*star* in B1), which appeared normal, tested negative (B2)

status of glioma tissue are time consuming, 60 min at least. This makes it difficult to test IDH1 mutation during the surgery. In order to solve this problem, we fabricated the immuno-wall devices with R132H mutant IDH1-specific capture antibody and performed immunoassay for a lysate of glioma tissue obtained from brain tumor patients. The total-IDH1 antibody was adopted as the detection antibody.

The representative immunoassay results for a glioma and its edge tissue are shown in Fig. 13.15. The fluorescence was observed only on the immuno-wall device used for the center of tumor, which means that we can define the boundary between the glioma and normal brain.

13.4 Summary

Microfluidic immunoassay devices have inherent advantages such as portability and reduced sample and reagent consumption. In addition, the microchannel can restrict molecular diffusion, resulting in the rapidity and high sensitivity of the immunoassay. We believe that these unique features allow us to use microfluidic immunoassay devices in the POC cancer diagnosis.

Here we have introduced the immuno-pillar devices and the immuno-wall devices. It has been demonstrated that these microfluidic immunoassay devices have great potential for practical immunoassay and POC cancer diagnostics. Also, the precision medicine and precision surgery have been realized. This implies that the microfluidic immunoassay devices have possibility of changing the process of diagnosis.

Acknowledgement This study was supported in part by the priority research project of "The knowledge hub of AICHI," Nagoya University Hospital Funding for Clinical Research, the Translational Research Network Program from the Japan Agency for Medical Research and Development (AMED), and JSPS KAKENHI Grant Number JP16K18438.

References

Arita H, Narita Y, Yoshida A, Hashimoto N, Yoshimine T, Ichimura K (2015) IDH1/2 mutation detection in gliomas. Brain Tumor Pathol 32:79–89

Asao T, Kumeda Y, Kawai T, Shibata T, Oda H, Haruki K, Nakazawa H, Kozaki S (2003) An extensive outbreak of staphylococcal food poisoning due to low-fat milk in Japan: estimation of enterotoxin A in the incriminated milk and powdered skim milk. Epidemiol Infect 130:33–40

Bange A, Halsall HB, Heineman WR (2005) Microfluidic immunosensor systems. Biosens Bioelectron 20:2488–2503

Chen RF, Knutson JR (1988) Mechanism of fluorescence concentration quenching of carboxyfluorescein in liposomes: energy transfer to nonfluorescent dimers. Anal Biochem 172:61–77

Chiem N, Harrison DJ (1997) Microchip-based capillary electrophoresis for immunoassays: analysis of monoclonal antibodies and theophylline. Anal Chem 69:373–378

Chin CD, Linder V, Sia SK (2007) Lab-on-a-chip devices for global health: past studies and future opportunities. Lab Chip 7:41–57

Delamarche E, Juncker D, Schmid H (2005) Microfluidics for processing surfaces and miniaturizing biological assays. Adv Mater 17:2911–2933

Ferlay J, Soerjomataram I, Dikshit R, Eser S, Mathers C, Rebelo M, Parkin DM, Forman D, Bray F (2015) Cancer incidence and mortality worldwide: sources, methods and major patterns in GLOBOCAN 2012. Int J Cancer 136:E359–E386

Gabay C, Kushner I (1999) Acute-phase proteins and other systemic responses to inflammation. N Engl J Med 340:448–454

Gervais L, Delamarche E (2009) Toward one-step point-of-care immunodiagnostics using capillary-driven microfluidics and PDMS substrates. Lab Chip 9:3330–3337

Gorovets D, Kannan K, Shen R, Kastenhuber ER, Islamdoust N, Campos C, Pentsova E, Heguy A, Jhanwar SC, Mellinghoff IK, Chan TA, Huse JT (2012) IDH mutation and neuroglial developmental features define clinically distinct subclasses of lower grade diffuse astrocytic glioma. Clin Cancer Res 18:2490–2501

Haes AJ, Terray A, Collins GE (2006) Bead-assisted displacement immunoassay for staphylococcal enterotoxin B on a microchip. Anal Chem 78:8412–8420

Hartmann C, Meyer J, Balss J, Capper D, Mueller W, Christians A, Felsberg J, Wolter M, Mawrin C, Wick W, Weller M, Herold-Mende C, Unterberg A, Jeuken JWM, Wesseling P, Reifenberger G, von Deimling A (2009) Type and frequency of IDH1 and IDH2 mutations are related to astrocytic and oligodendroglial differentiation and age: a study of 1,010 diffuse gliomas. Acta Neuropathol 118:469–474

Henares TG, Mizutani F, Hisamoto H (2008) Current development in microfluidic immunosensing chip. Anal Chim Acta 611:17–30

Horbinski C (2013) What do we know about IDH1/2 mutations so far, and how do we use it? Acta Neuropathol 125:621–636

Hosokawa K, Omata M, Sato K, Maeda M (2006) Power-free sequential injection for microchip immunoassay toward point-of-care testing. Lab Chip 6:236–241

Ihara M, Yoshikawa A, Wu Y, Takahashi H, Mawatari K, Shimura K, Sato K, Kitamori T, Ueda H (2010) Micro OS-ELISA: rapid noncompetitive detection of a small biomarker peptide by open-sandwich enzyme-linked immunosorbent assay (OS-ELISA) integrated into microfluidic device. Lab Chip 10:92–100

Ikami M, Kawakami A, Kakuta M, Okamoto Y, Kaji N, Tokeshi M, Baba Y (2010) Immuno-pillar chip: a new platform for rapid and easy-to-use immunoassay. Lab Chip 10:3335–3340

Jin W, Yamada K, Ikami M, Kaji N, Tokeshi M, Atsumi Y, Mizutani M, Murai A, Okamoto A, Namikawa T, Baba Y, Ohta M (2013) Application of IgY to sandwich enzyme-linked immunosorbent assays, lateral flow devices, and immunopillar chips for detecting staphylococcal enterotoxins in milk and dairy products. J Microbiol Methods 92:323–331

Kakuta M, Takahashi H, Kazuno S, Murayama K, Ueno T, Tokeshi M (2006) Development of the microchip-based repeatable immunoassay system for clinical diagnosis. Meas Sci Technol 17:3189

Kasama T, Hasegawa Y, Kondo H, Ozawa T, Kaji N, Tokeshi M, Baba Y (2014) Development of immuno-wall devices and a mobile fluorescence reader for on-site sample-to-answer immunoassay. In: Proceedings of international conference on miniaturized systems for chemistry and life sciences, pp 935–937

Kasama T, Ikami M, Jin W, Yamada K, Kaji N, Atsumi Y, Mizutani M, Murai A, Okamoto A, Namikawa T, Ohta M, Tokeshi M, Baba Y (2015a) Rapid, highly sensitive, and simultaneous detection of staphylococcal enterotoxins in milk by using immuno-pillar devices. Anal Methods 7:5092–5095

Kasama T, Hase T, Nishiwaki N, Yogo N, Sato M, Kondo M, Kaji N, Tokeshi M, Hasegawa Y, Baba Y (2015b) Immuno-wall lab-on-chip companion diagnostic devices for rapid and low-cost detection of mutant epidermal growth factor receptors (EGFR) from cytological samples in lung cancer patients. In: Proceedings of international conference on miniaturized systems for chemistry and life sciences, pp 925–927

Kuang H, Wang W, Xu L, Ma W, Liu L, Wang L, Xu C (2013) Monoclonal antibody-based sandwich ELISA for the detection of staphylococcal enterotoxin A. Int J Environ Res Public Health 10:1598–1608

Linder V, Sia SK, Whitesides GM (2005) Reagent-loaded cartridges for valveless and automated fluid delivery in microfluidic devices. Anal Chem 77:64–71

Lynch TJ, Bell DW, Sordella R, Gurubhagavatula S, Okimoto RA, Brannigan BW, Harris PL, Haserlat SM, Supko JG, Haluska FG, Louis DN, Christiani DC, Settleman J, Haber DA (2004) Activating mutations in the epidermal growth factor receptor underlying responsiveness of non-small-cell lung cancer to gefitinib. N Engl J Med 350:2129–2139

Moorthy J, Mensing GA, Kim D, Mohanty S, Eddington DT, Tepp WH, Johnson EA, Beebe DJ (2004) Microfluidic tectonics platform: a colorimetric, disposable botulinum toxin enzyme-linked immunosorbent assay system. Electrophoresis 25:1705–1713

Ohashi T, Mawatari K, Sato K, Tokeshi M, Kitamori TA (2009) micro-ELISA system for the rapid and sensitive measurement of total and specific immunoglobulin E and clinical application to allergy diagnosis. Lab Chip 9:991–995

Paez JG, Jänne PA, Lee JC, Tracy S, Greulich H, Gabriel S, Herman P, Kaye FJ, Lindeman N, Boggon TJ, Naoki K, Sasaki H, Fujii Y, Eck MJ, Sellers WR, Johnson BE, Meyerson M (2004)

EGFR mutations in lung cancer: correlation with clinical response to gefitinib therapy. Science 304:1497–1500

Parsons DW, Jones S, Zhang X, Lin JC-H, Leary RJ, Angenendt P, Mankoo P, Carter H, Siu I-M, Gallia GL, Olivi A, McLendon R, Rasheed BA, Keir S, Nikolskaya T, Nikolsky Y, Busam DA, Tekleab H, Diaz LA, Hartigan J, Smith DR, Strausberg RL, Marie SKN, Shinjo SMO, Yan H, Riggins GJ, Bigner DD, Karchin R, Papadopoulos N, Parmigiani G, Vogelstein B, Velculescu VE, Kinzler KW (2008) An integrated genomic analysis of human glioblastoma multiforme. Science 321:1807–1812

Rose SA, Bankes P, Stringer MF (1989) Detection of staphylococcal enterotoxins in dairy products by the reversed passive latex agglutination (SET-RPLA) kit. Int J Food Microbiol 8:65–72

Rosell R, Moran T, Queralt C, Porta R, Cardenal F, Camps C, Majem M, Lopez-Vivanco G, Isla D, Provencio M, Insa A, Massuti B, Gonzalez-Larriba JL, Paz-Ares L, Bover I, Garcia-Campelo R, Moreno MA, Catot S, Rolfo C, Reguart N, Palmero R, Sánchez JM, Bastus R, Mayo C, Bertran-Alamillo J, Molina MA, Sanchez JJ, Taron M, Group SLC (2009) Screening for epidermal growth factor receptor mutations in lung cancer. N Engl J Med 361:958–967

Sato K, Tokeshi M, Odake T, Kimura H, Ooi T, Nakao M, Kitamori T (2000) Integration of an immunosorbent assay system: analysis of secretory human immunoglobulin A on polystyrene beads in a microchip. Anal Chem 72:1144–1147

Sato K, Tokeshi M, Kimura H, Kitamori T (2001) Determination of carcinoembryonic antigen in human sera by integrated bead-bed immunoasay in a microchip for cancer diagnosis. Anal Chem 73:1213–1218

Sato K, Yamanaka M, Takahashi H, Tokeshi M, Kimura H, Kitamori T (2002) Microchip-based immunoassay system with branching multichannels for simultaneous determination of interferon-γ. Electrophoresis 23:734–739

Sato K, Yamanaka M, Hagino T, Tokeshi M, Kimura H, Kitamori T (2004) Microchip-based enzyme-linked immunosorbent assay (microELISA) system with thermal lens detection. Lab Chip 4:570–575

Sequist LV, Bell DW, Lynch TJ, Haber DA (2007) Molecular predictors of response to epidermal growth factor receptor antagonists in non-small-cell lung cancer. J Clin Oncol 25:587–595

Shin K-S, Lee SW, Han K-C, Kim SK, Yang EK, Park JH, Ju B-K, Kang JY, Kim TS (2007) Amplification of fluorescence with packed beads to enhance the sensitivity of miniaturized detection in microfluidic chip. Biosens Bioelectron 22:2261–2267

Sung W-C, Chen H-H, Makamba H, Chen S-H (2009) Functionalized 3D-hydrogel plugs covalently patterned inside hydrophilic poly(dimethylsiloxane) microchannels for flow-through immunoassays. Anal Chem 81:7967–7973

Suzuki H, Aoki K, Chiba K, Sato Y, Shiozawa Y, Shiraishi Y, Shimamura T, Niida A, Motomura K, Ohka F, Yamamoto T, Tanahashi K, Ranjit M, Wakabayashi T, Yoshizato T, Kataoka K, Yoshida K, Nagata Y, Sato-Otsubo A, Tanaka H, Sanada M, Kondo Y, Nakamura H, Mizoguchi M, Abe T, Muragaki Y, Watanabe R, Ito I, Miyano S, Natsume A, Ogawa S (2015) Mutational landscape and clonal architecture in grade II and III gliomas. Nat Genet 47:458–468

Tachi T, Kaji N, Tokeshi M, Baba Y (2007) Microchip-based immunoassay. Bunseki Kagaku 56:521

Thompson JA, Bau HH (2010) Microfluidic, bead-based assay: theory and experiments. J Chromatogr B 878:228–236

Wild D (2005) The immunoassay handbook. Elsevier, Amsterdam

Yamamichi A, Kasama T, Ohka F, Suzuki H, Kato A, Motomura K, Hirano M, Ranjit M, Chalise L, Kurimoto M, Kondo G, Aoki K, Kaji N, Tokeshi M, Matsubara T, Senga T, Kaneko MK, Suzuki H, Hara M, Wakabayashi T, Baba Y, Kato Y, Natsume A (2016) An immuno-wall microdevice exhibits rapid and sensitive detection of IDH1-R132H mutation specific to grade II and III gliomas. Sci Technol Adv Mater 17:18–625

Zubtsov D, Ivanov S, Rubina A, Dementieva E, Chechetkin V, Zasedatelev A (2006) Effect of mixing on reaction-diffusion kinetics for protein hydrogel-based microchips. J Biotechnol 122:16–27